Splitting-crack propagation in pullout tests

P. Lura
Delft University of Technology, Delft, The Netherlands

G.A. Plizzari & P. Riva
University of Brescia, Brescia, Italy

ABSTRACT: Although several experimental results on bond strength are available and splitting represents an important aspect of bond, only few studies have dealt with splitting-crack development. Splitting is a 3D phenomenon but only splitting-crack opening on concrete surface can easily be measured. Accordingly, Finite Element analysis could help understanding splitting-crack development and bond behavior. However, FE studies are limited by the difficulty of correctly modeling bond. Main purpose of this research work is to develop a simple 3D interface FE model that could be used as a tool for establishing design criteria for anchorages and splices. Such a model is validated by simulating a set of experimental pull-out tests, representing an anchored deformed bar in the influence zone of one single stirrup along a splitting crack. Both bond-slip curve and splitting-crack opening could be modeled with good reliability. In spite of its simplicity, the proposed model provides a basis for studying more complex structural configurations.

1 INTRODUCTION

In R.C. structures, splitting of concrete surrounding a rebar occurs when the radial stresses induced by wedge action of the ribs exceed concrete tensile strength (Tepfers 1973, Fig. 1).
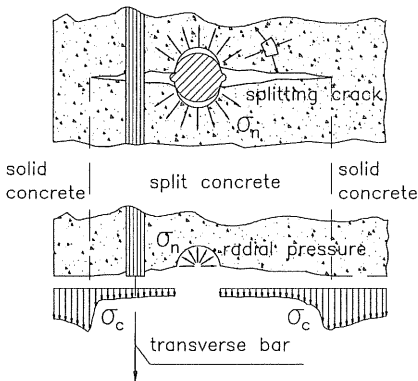

Figure 1. Splitting crack and confining actions around a ribbed bar (Giuriani 1981).

Bond behavior can be correctly studied only if splitting and confinement of concrete are taken into account (Gambarova et al. 1989, Giuriani et al. 1991). In anchorages with low confinement, splitting cracks may develop under service loads (Plizzari et al. 1996). Since splitting cracks propagate longitudinally along the bar and a considerable length of the

reinforcing bar (rebar) may be exposed to aggressive agents, the role of splitting in impairing structural durability should also be considered (Giuriani & Plizzari 1998).

Although splitting is widely recognized as an important aspect of bond (FIB 2000), only a few studies have been published on splitting-crack development. As a consequence, scant attention has been given by present building codes to splitting control in both anchorages and splices.

The 3D development of splitting crack can hardly be determined in laboratory tests where splitting-crack opening is measured on the concrete surface. Consequently, important data concerning durability of a structure with splitting cracks are lost. For example, splitting-crack opening at the bar interface, which is of major interest for bar corrosion, is not measured in usual experimental tests.

In Finite Element studies, a perfect bond (no slip) has often been assumed between a rebar and concrete. In other cases, bond has been treated as an interface phenomenon governed by a relation between the shear stress and the bar-to-concrete slip (Yankelevsky 1985). However, since several structural phenomena take place around a ribbed bar, true constitutive laws can hardly be introduced (Gambarova & Giuriani 1985, Gerstle & Ingraffea 1990). In order to correctly model bond behavior, the characteristics of concrete, reinforcing bars, and steel-to-concrete interface should be considered.

Van Mier & Vervuurt (1995) modeled the con-

crete layer close to the bar by using a "lattice model", which is a micromechanics-based model.

Reinforcing bars have also been treated with discrete, embedded or smeared models (ASCE 1982), with linear elastic behavior or including bar yielding (Bigaj et al. 1996).

Since bond behavior depends mainly on the mechanical interaction between the ribs and surrounding concrete, the key-point in bond modeling is steel-to-concrete interface. This interface has been modeled by means of an explicit discretization of the bar ribs (Reinhardt et al. 1984, Ozbolt & Eligehausen 1992). However, since the aggregates are larger than the ribs, modeling concrete as a homogeneous material is only a rough idealization. In order to take into account both slip and wedge action, some researchers used linear or nonlinear springs between the rebar and the surrounding concrete (Morita & Fujii 1985, Keuser & Mehlhorn 1987).

Most of the approaches described above were implemented in research-oriented codes and were often based on an axisymmetric mesh with splitting crack developing radially from the deformed bar. These models might not be adequate to study splitting phenomena in a real structure, where, due to the reinforcement arrangement and rib geometry, splitting cracks tend to develop in preferential planes (Plizzari, Klink & Slowik 1998, Fig. 1).

The main purpose of this research work is to study the 3D splitting-crack development to provide useful information for structural durability. This was obtained by means of a 3D FE model, developed within the framework of the commercially available code DIANA (1996). The proposed model was validated by simulating a series of experimental pull-out tests on rebars in prisms of plain and steel fiber reinforced concrete with and without stirrups (Plizzari 1999).

2 INTERFACE MODEL

The model was implemented in the FE code DIANA V.6.2. The correct transmission of longitudinal and transverse forces between the bar and the surrounding concrete represents the key point in the FE simulation. The interface elements available in DIANA cannot deal with the transversal forces radiating from the bar to the concrete and, contrary to the experimental evidence, cannot model splitting-crack growth. Therefore, a different strategy had to be adopted as illustrated in the following.

The main mechanism of force transfer between a pulled bar and the surrounding concrete is related to the wedge action exerted by the crushed concrete in front of the bar (Fig. 3a). The mechanism related to such behavior is illustrated in Figure 3b. When a bar is pulled, a point C in the concrete, initially coincident with a point S on the rebar, is forced to move

away from S towards point C' sliding along an inclined surface characterized by an angle θ that varies during the loading history (Fig. 3a). In a FE analysis, this mechanism could be conveniently modeled by introducing a kinematic relationship between the displacements $\mathbf{u_S}$ of a bar node and the displacements $\mathbf{u_C}$ of a neighboring concrete node.
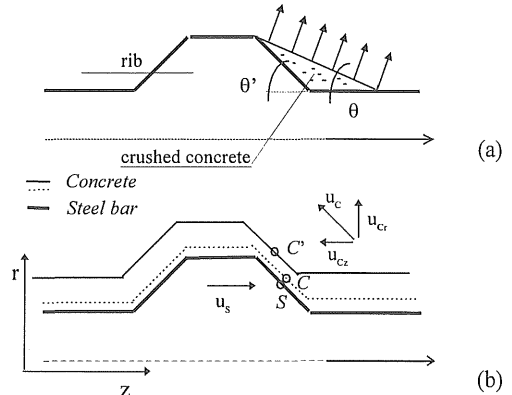

Figure 3. Mechanism of force transmission between ribs and surrounding concrete (a); kinematic relationship between ribs and surrounding concrete (b).

This approach was used in the present model, developed within DIANA 6.2, where table TYINGS offers the possibility to link general displacements of a set of "slave" nodes to the displacements of a "master" node (option FIXED). The kinematic relationship adopted consists in forcing a concrete node to move in the radial direction proportionally to the longitudinal displacement of the corresponding rebar node (Figs 3 and 4), i.e.:

$$\mathbf{u_C} = \alpha \cdot \mathbf{u_S} \qquad (1)$$

Even though parameter α varies during the test, due to concrete crushing, a constant value was assumed, according to the best fitting of several experimental results obtained by Plizzari (1999).

The rebar has been modeled by means of 8 nodes hexahedral elements and the aforementioned kinematic constraint has been applied only to the nodes corresponding to the rib location (points A and B in Figs 4 and 5). The displacements on the symmetry plane have been left unconstrained (point C).
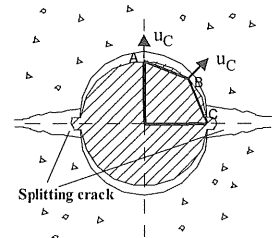

Figure 4. Kinematic relationship between ribs and surrounding concrete: finite element idealization, plane view.
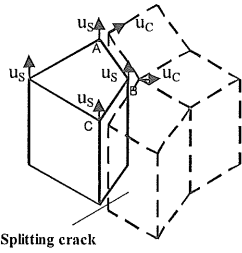
Figure 5. Kinematic relationship between ribs and surrounding concrete: finite element idealization, three-dimensional view.

3 SPECIMEN DESCRIPTION

The splitting-crack propagation was studied by applying the described kinematic relationship to the FE analysis of some pull-out tests performed at the University of Brescia (Plizzari 1999). The tests concern φ24 deformed bars embedded for 200 mm in concrete prisms representing the influence zone of a stirrup present along an anchored bar (Fig. 6). The concrete prism dimensions were 400x120x200 mm. Transverse reinforcement made of two φ8 bars was introduced in some specimens to simulate the confining action of a two-legged stirrup. Since a beam with usual concrete covers and closely spaced rebars exhibits concrete splitting in planes containing the bars, the anchored bar was placed with the two ribs oriented towards concrete blocks C1 and C2, forcing plane AA to be the preferential plane for the splitting-crack formation. Two separate reaction plates allowed the main splitting crack to form and develop freely (Plizzari et al. 1998, Fig. 7). Four steel angles were placed in the splitting-crack plane, on the top and bottom sides of the specimen, to act as crack initiators (Fig. 6). Because of these angles, concrete confinement was active only in the middle zone (150 mm) of the embedded length. Further details on the experimental set-up can be found in Plizzari (1999).

The specimens analyzed are listed in Table 1. Owing to the presence of two planes of symmetry, only a quarter of the specimen was modeled. A 3D mesh of linear hexahedral elements (elements type HX24L in DIANA) was used to represent both the concrete and the steel bar (Figs 7 and 8).

Table 1. Materials and stirrup diameter of the specimens considered in the FE analysis

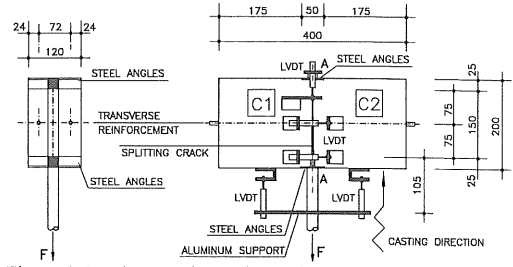| Specimen	Material	Stirrup diameter (mm)
N4B4	Normal Strength Concrete (NSC)	No stirrups
8N4B4	Normal Strength Concrete (NSC)	8
H4B4	High Strength Concrete (HSC)	No stirrups
8H4B4	High Strength Concrete (HSC)	8
NS4B4	NSC with steel fibers (NSC-SFR)	No stirrups
HS4B4	HSC with steel fibers (HSC-SFR)	No stirrups

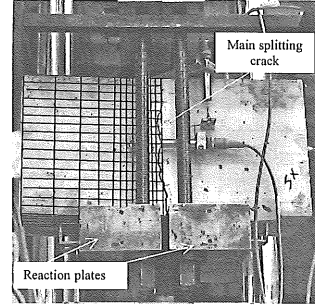Figure 6. Specimen and experimental set-up.

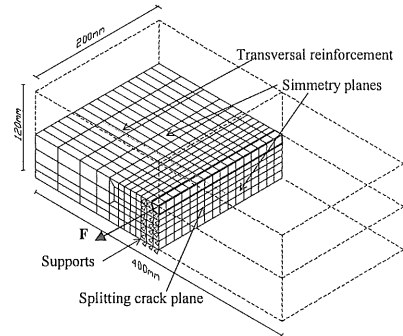Figure 7. Picture of the specimen with superimposed FE mesh.

Figure 8. Three-dimensional FE mesh.

4 MATERIAL PROPERTIES

The numerical analyses were performed on specimens made with normal and high strength concrete (NSC and HSC, respectively), with and without hooked steel fibers (φ=0.5 mm, l=30 mm, l/φ=60). The volume fraction (V_f) of steel fibers was equal to 0.38% for both normal and high-strength concrete.

4.1 Concrete

The tensile strength (f_{ct}), fracture energy (G_F), and compressive strength ($f_{c,cube}$) values of concrete are shown in Table 2. These values are based on tests performed on the same mixes used in the pull-out tests. A Poisson's coefficient v_c=0.2 was used in all the analyses.

Table 2. Mechanical properties of the materials used in the FE analyses.

Specimen	E_c [MPa]	$f_{c,cube}$ [MPa]	f_c^* [MPa]	f_{ct} [MPa]	G_f [J/m²]
NSC	30,000	44	37.4	3.87	138
NSC-SFR	30,000	50	42.5	4.09	2288
HSC	49,000	77	65.5	4.96	133
HSC-SFR	49,000	85	72.3	5.45	898

* f_c calculated from $f_{c,cube}$ according to CEB-FIP MC 1990.

The material's yield surface was described by means of a Drucker-Prager yield condition in compression, combined with a Galileo-Rankine criterion in tension, with a smeared-crack approach based on a cohesive-crack model to simulate the behavior of concrete in tension after cracking.

Since the response in a pull-out test is dominated by splitting and cracking of concrete in tension, with concrete in compression remaining in the elastic range, the behavior in compression was assumed to be elastic-perfectly plastic, with associated plasticity and an internal friction angle $\varphi = \psi = 11.5°$, as suggested by Feenstra and De Borst (1995).

Concrete tensile behavior is assumed to be linear up to the tensile strength. For both NSC and HSC, the post-peak behavior in tension is described by the Hordijk's cohesive-crack law (Hordijk 1991, Fig. 9). In the case of fiber reinforced concrete (NSC-SFR and HSC-SFR), the experimental evidence on the same materials has shown that the model proposed by Stang (1992) is well suited for describing the post-peak branch (Fig. 9). Thereby, being Stang's model not implemented in DIANA, a poli-linear approximation has been used in the analyses.
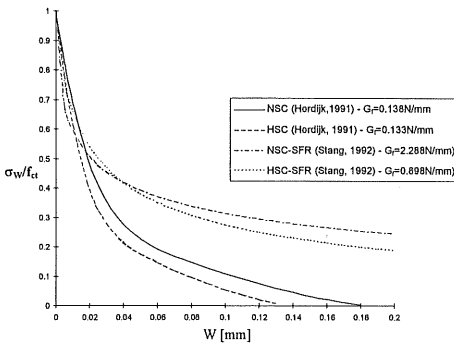

Figure 9. Softening branch in tension for interface elements according to Hordijk (1991) model (for NSC and HSC), and according to Stang (1992) model (for NSC-SFR and HSC-SFR).

4.2 Interface elements (discrete crack)

Being the splitting-crack plane known a-priori from the experimental set-up (Figs 7 and 8), a discrete-crack approach was adopted for the main splitting crack. Accordingly, 8 node plane interface elements (element type Q24IF in DIANA) have been used to model the splitting crack. Only mode I crack open-

ing was taken into account, as observed in the tests. To simulate the discontinuity caused by the steel angles, the concrete tensile strength at both ends of the interface layer was assumed equal to zero.

After cracking, the interface behavior follows a softening branch (Fig. 9). It is noted that, having modeled only one of the concrete blocks separated by the splitting crack, only half of the total fracture energy is dissipated by the interface elements in the analyses.

4.3 Reinforcing bar

Since yielding of the principal bar was not observed during the tests, the steel was modeled as a linear elastic material, with E_s=210,000 MPa and ν_s=0.3.

4.4 Stirrups

Only two specimens had stirrups, which were modeled by means of perfectly embedded reinforcing bars (table REINFO in DIANA) with no degrees of freedom. Since DIANA does not allow to embed bars in interface elements (8N4B4 and 8H4B4), while the stirrups had to pass through the splitting plane (i.e. through the interface elements), it was necessary to remove the interface element corresponding to the reinforcement location. This is equivalent to impose a zero opening of the discrete crack at the stirrups location, as if no slip may occur between the stirrups and the concrete across the splitting crack. This is an obvious limitation of the approach. However, a partial compensation to the lack of slip across the splitting plane is given by the deformation of the nearby brick elements which show somewhat higher deformations due to smeared cracking than the remaining elements.

The stirrup steel is modeled as an elastic perfectly plastic material, with E_s=210,000 MPa, ν_s=0.3, and yielding strength f_{sy}=538 MPa, as observed in the tensile tests performed on the stirrups.

5 RESULTS

The nonlinear analyses were performed by imposing an increasing relative displacement (δ_L) of the nodes at one end of the steel bar with respect to the concrete matrix, as in the tests (Plizzari 1999). The reaction at the bar nodes corresponds to the value of the pull-out force (F) which varies with the bar slip. The pull-out force is balanced by the reaction of the restraints on the upper face of the specimen (Fig. 8). Although not explicitly included in the model, the effects of microcracking and concrete crushing are implicitly taken into account through the imposed kinematic relation and the non-linear behavior of the concrete elements surrounding the bar.

At each step of the analysis, an incremental-

iterative scheme was used by adopting a constant stiffness matrix throughout the analysis; i.e. the stiffness matrix was calculated only once, at the first step, and was kept constant in the following steps. This procedure, though slower than others (regular or Modified Newton-Raphson), has proved to be much more stable and the convergence was reached also in strongly nonlinear situations (cracking of both the interface elements and concrete matrix).

After several numerical simulations, the value $\alpha=0.5$ was found to give the best fit. Accordingly, the kinematic relation between the radial displacement of a concrete node and the tangential displacement of a corresponding reinforcement node was taken as:

$$\mathbf{u}_C = 0.5 \cdot \mathbf{u}_S \qquad (2)$$

Experimental and numerical force-slip (F-δ_L) diagrams for three of the specimens analyzed are shown in Figures 10-12. The results concerning the other specimens may be found in Lura et al. (2001). The FE model correctly represents the experimental behavior for all concrete types considered. In particular, both the initial anchorage stiffness and the nonlinear behavior (including the post-peak branch) are well represented. In fact, the differences between the experimental and numerical curves are generally smaller than ±30%, which is satisfactory compared to the complexity of the structural mechanisms present around a ribbed bar and to the experimental scatter systematically observed in bond tests.

The results in Figures 10 and 11 also show that stirrups have the effect of increasing considerably both anchorage strength and maximum slip in NSC
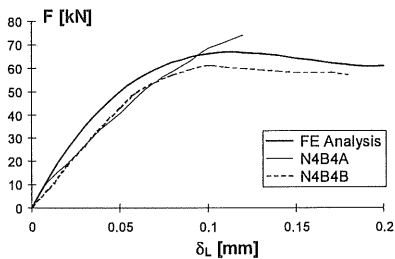

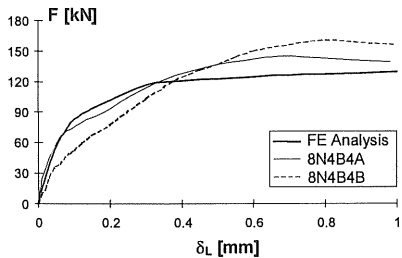Figure 10. F-δ_L curves for specimen N4B4 (NSC).

Figure 11. F-δ_L curves for specimen 8N4B4 (NSC, ϕ8 stirrup).

specimens. In particular, a maximum pull-out force (F_{max}) lower than 70 kN and a slip of only 0.2 mm is obtained before the splitting failure of an unconfined specimen, whereas F_{max} higher than 120 kN and a slip as high as 1 mm is observed in specimens with stirrups.
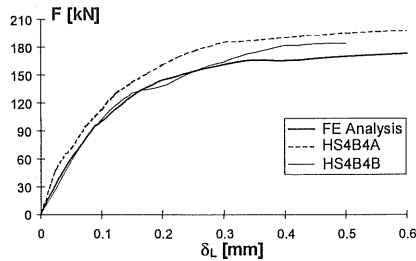

Figure 12. F-δ_L curves fore specimen HS4B4 (HSC-SFR).

The introduction of steel fibers in the concrete mix has an effect similar to the presence of stirrups. In fact, Figure 12 shows that a ductile behavior may be obtained even for HSC, which is in principle more brittle than NSC, by adopting a small fraction of steel fibers (V_f=0.38%). In this case, a maximum pull-out force of approximately 180 kN and a maximum slip close to 0.6 mm were observed.

Figures 13-15 show the splitting-crack width, measured on the concrete surface at the mid point of the embedded length (Fig. 6), as a function of the imposed displacement (δ_L), for the same three specimens. In particular, Figure 13 shows that for unconfined specimens the splitting-crack opening occurs in a sudden and unstable manner for δ_L approximately equal to 0.1 mm, whereas for specimens reinforced with either stirrups or steel fibers the splitting-crack opening develops in a stable and almost linear manner for increasing imposed bar slip (Figs 14 and 15).

Figure 16 shows the numerical bond stress distribution along the embedded length of the principal bar in specimen N4B4. For low slip values (δ_L=0.01 mm), the bond stress decreases gradually from the pulled to the free bar end, while, for larger slip values (δ_L=0.1 mm and δ_L=0.2 mm), high bond stresses localize close to the pulled end.

Figures 17 and 18 exhibit the bond stress distribution along the embedded length of the principal bar in specimens 8N4B4 and HS4B4, respectively. In particular, Figure 17 shows that for low slip values (δ_L=0.01 mm), the bond stress decreases gradually from the pulled to the free bar end while, for larger slip values (δ_L=0.5 mm), high bond stresses localize close to the pulled end. Being the anchorages confined by a transversal bar, bond localization is observed also next to the stirrup (x=100 mm), where the local confinement is higher and the splitting-crack width smaller. In the post-peak range (δ_L=1.0 mm), the bond stress distribution does not
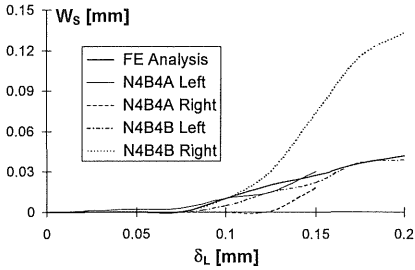
Figure 13. Splitting-crack width for specimens N4B4 (NSC without stirrups).
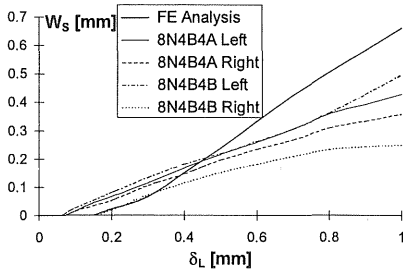

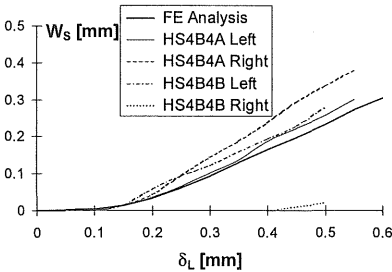Figure 14. Splitting-crack width for specimens 8N4B4 (NSC, $\phi 8$ stirrup).

Figure 15. Splitting-crack width for specimens HS4B4 (HSC-SFR without stirrups).

significantly change any longer.

Figure 18 shows that, for low slip values ($\delta_L = 0.01$ mm), the bond stress distribution along the bar in the HSC-SFR specimen is similar to that of specimen 8N4B4 with transverse reinforcement. For larger slip values ($\delta_L = 0.3$ mm), a high bond stress localization is again observed at the pulled bar end, with the remaining part of the bar showing an almost uniform bond stress distribution. In the post-peak range ($\delta_L = 0.6$ mm), the bond stress distribution becomes more uniform. Owing to the presence of steel fibers, the anchorage exhibits a ductile behavior and the splitting crack propagates across the whole section before failure.

While in the tests the splitting-crack opening (w_S) could be measured only along the outer surface, in the numerical analyses the crack opening could be determined everywhere over the splitting-crack sur-

face. Such opening was defined as twice the crack opening in the discrete-crack plane plus the integral of the smeared-crack deformations over the first layer of finite elements (thickness equal to 8.65 mm).

Figures 19-21 exhibit a 3D representation of the crack distribution over the splitting plane for specimens N4B4, 8N4B4, and HS4B4, respectively. In all figures the pulled bar end is located to the left side, indicated by an arrow.

Figures 19a and b show that, in specimen N4B4 (NSC without stirrups) the splitting crack localizes near the pulled bar, showing a negligible propagation across the splitting plane. When the traction free crack opening near the bar is reached (0.18 mm for NSC without fibers, Fig. 9), the pulled bar is no longer constrained and the anchorage's collapse is observed.
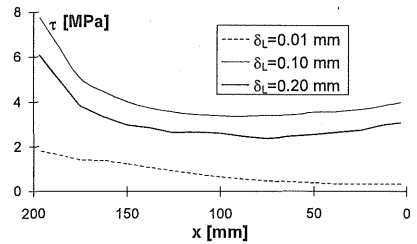

Figure 16. Bond stress distribution along the bar for different values of the bar slip. Specimen N4B4 (NSC without stirrups).
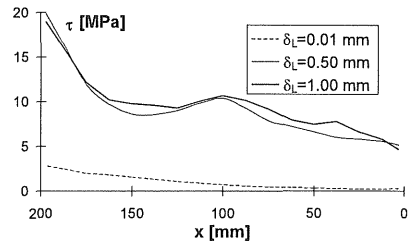

Figure 17. Bond stress distribution along the bar for different values of the bar slip. Specimen 8N4B4 (NSC, $\phi 8$ stirrup).
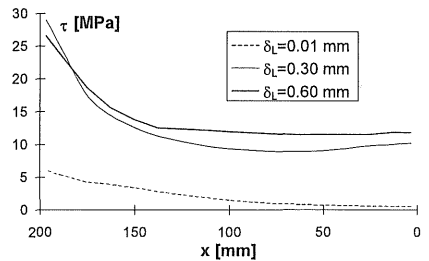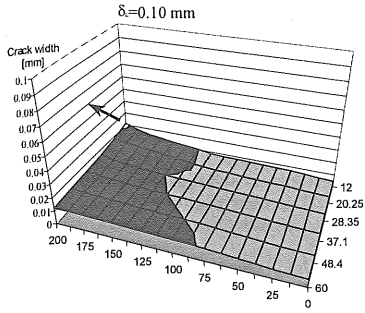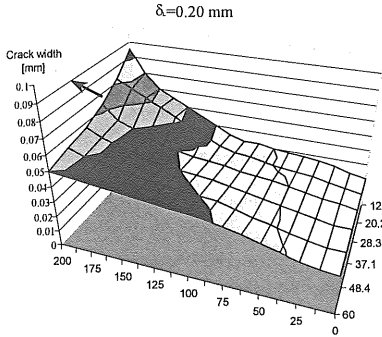

Figure 18. Bond stress distribution along the bar for different values of the bar slip. Specimen HS4B4 (HSC-SFR without stirrups).
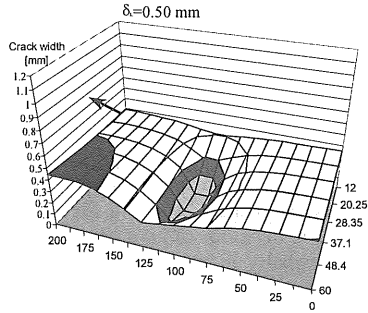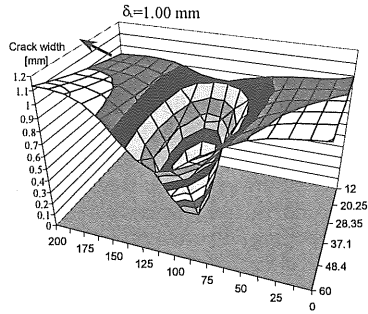
1004

δ_L=0.10 mm

Crack width [mm]

(a)

δ_L=0.20 mm

Crack width [mm]

(b)

Figure 19. Splitting crack distribution for specimen N4B4 (NSC without stirrups): (a) δ_L = 0.1 mm; (b) δ_L = 0.2 mm.

δ_L=0.50 mm

Crack width [mm]

(a)

δ_L=1.00 mm

Crack width [mm]

(b)

Figure 20. Splitting crack distribution for specimen 8N4B4 (NSC with φ8 stirrups): (a) δ_L = 0.5mm; (b) δ_L = 1 mm.

Figures 20a and b show that, in specimen 8N4B4 (NSC with φ8 stirrup), the region next to the transversal bar is the one with the smallest splitting-crack width. For large slip values, the crack width next to the stirrup remains very low, while the rest of the section is wholly cracked. The confining action of the cracked concrete is still active in a large part of the specimen under service conditions (Fig. 20a). In fact, the splitting-crack opening is smaller than the traction-free crack opening in a significant part of the split concrete and cohesive stresses may be transmitted across the crack faces. The confining action of cracked concrete is no longer present at the ultimate state, when confinement is provided only by stirrups (Fig. 20b).

Figures 21a and b show that, in specimen HS4B4 (HSC-SFR without stirrups) larger crack openings are observed near the pulled and free edges of the specimen, where the confinement due to the surrounding concrete is missing. The splitting crack tends to propagate across the splitting plane, and a less significant localization is observed than for specimen N4B4. Due to an increased traction-free crack opening (Fig. 9) in SFR concrete, stress transfer is possible in the whole splitting plane under both service and ultimate loads. The small crack width over most of the splitting plane protects the bar in an aggressive environment and thus improves structural durability.
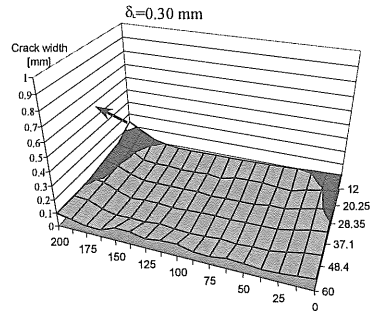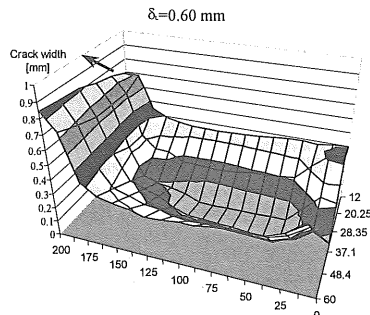

δ_L=0.30 mm

Crack width [mm]

(a)

δ_L=0.60 mm

Crack width [mm]

(b)

Figure 21. Splitting crack distribution for specimen HS4B4 (HSC-SFR): (a) δ_L = 0.3 mm; (b) δ_L = 0.6 mm.

6 CONCLUDING REMARKS

A simple interface element for bond, based on a kinematic relationship between the relative displacement of the bar and the surrounding concrete, was proposed.

The comparison between experimental and numerical results showed that, by using the proposed interface model, the behavior of an anchored bar can be modeled realistically in terms of both bond-slip curve and splitting-crack opening.

The same kinematic relationship was used for all concrete mixes and geometric conditions. This fact implies that the variations in the observed anchorage behavior are due only to the different materials properties and to the presence of transverse reinforcement. Thus, the model allows not only to describe but also to predict the behavior of a number of different solutions for the design of anchorages.

The model herein presented allowed to study the actual bond distribution along an anchorage and the splitting-crack opening distribution in the crack plane. The numerical results show the importance of stirrups in improving bond strength and the benefit of steel fibers, which make bond behavior very ductile even in specimens without transverse reinforcement. Furthermore, by reducing the splitting-crack opening, steel fibers increase bond strength and improve structural durability.

REFERENCES

ASCE 1982. *State-of-the-Art Report on Finite Element Analysis of Reinforced Concrete*, Chapter 3 Modeling of Reinforcement and Representation of Bond, Task Committee FE Analysis of R/C Structures, Chairman Nilson A.H.: 149-203.

Bigaj, A.J., Den Uijl, J.A. & Walraven, J.C. 1996. A bond model for ribbed bars in HSC and NSC: an experimental study. *Proc. 4th intern. symp. on the Utilization of High-Strength/High-Performance Concrete, Paris*: 1125-1134.

DIANA-Finite Element Analysis 1996. *User's Manual*. TNO Building and Construction Research, P.O. Box 49, 2600 AA Delft, The Netherlands.

Feenstra, P. & De Borst, R. 1995. A composite plasticity model for concrete. *International Journal of Solids and Structures* 33(5): 707-730.

FIB 2000. *Bond of reinforcement in concrete*, Chapter 1 Bond Mechanics Including Pull-out and Splitting Failures. FIB Bulletin 10.

Gambarova, P.G. & Giuriani, E. 1985. Discussion of "Study of transfer of tensile forces by bond", by D.H. Jiang, S.P. Shah, A.T. Andonian. *ACI Journal* 82(3): 381-383.

Gambarova P.G., Rosati G.P. & Zasso B. 1989. Steel-concrete bond after concrete splitting: (I) test results; (II) constitutive laws and interface deterioration. *Materials and Structures* 22: 35-47 and 347-356.

Gerstle, W.H. & Ingraffea, A.R. 1990. Does Bond-Slip Exist? *Micromechanics of Failure of Quasi-Brittle Materials; Proc. intern. conf., Albuquerque (NM, USA)*: 407-416.

Giuriani, E. 1981. Experimental investigation on the bond-slip law of deformed bars in concrete. *IABSE Colloquium on Advanced Mechanics of Reinforced Concrete, Delft, The Netherlands*: 121-142.

Giuriani, E. & Plizzari, G.A. 1998. Interrelation of splitting and flexural cracks in R.C. beams. *ASCE Journal of Structural Engineering* 124(9): 1032-1040.

Hordijk, D.A. 1991. *Local approach to fatigue of concrete*. Ph.D. Thesis, Delft University of Technology, The Netherlands.

Keuser, M. & Mehlhorn, G. 1987. Finite element models for bond problems. *ASCE Journal of Structural Engineering* 113(10): 2160-2173.

Lura, P., Plizzari, G.A. & Riva, P. 2001. Finite Element Analysis of pull-out tests. Submitted to *Magazine of Concrete Research*.

Morita S. & Fujii S. 1985. Bond-Slip Models in Finite Element Analysis. *Finite Element Analysis of Reinforced Concrete Structures*, ASCE, 348-363.

Ozbolt, J. & Eligehausen, R. 1992. Numerical Simulation of Cycling Bond-Slip Behavior. *Bond in Concrete: from Research to Practice; Proc. intern. conf., CEB-RTU (Riga Technical University), Riga (Latvia)*: 12.27-12.33.

Plizzari, G. 1999. Bond and splitting crack development in normal and high-strength fiber-reinforced concrete. *13th Eng. Mechanics Division Conference – EMD99, Baltimore (MD, USA)*, on CD ROM support.

Plizzari, G.A., Cangiano, S. & Cere, N. 2000. Post-peak behavior of fiber reinforced concrete under cyclic tensile loads. *ACI Materials Journal 97(2)*: 182-192.

Plizzari, G.A., Deldossi, M.A. & Massimo, S. 1998. Transverse reinforcement effects on anchored deformed bars. *Magazine of Concrete Research* 50(2): 161-177.

Plizzari, G.A., Klink, T. & Slowik, V. 1998. Investigation into the failure of concrete rings under inner pressure. *FRAMCOS3, Mihashi H. ed., Aedificatio, Gifu (Japan), October 12-16*: 1311-1320.

Reinhardt, H.W., Blaauwendraad, J. & Vos, E. 1984. Prediction of bond between steel and concrete by numerical analysis. *Materials and Structures* 17(100): 311-320.

Stang, H. 1992. Evaluation of properties of cementitious fiber composite materials. In Reinhardt and Naaman (eds), *High Performance Fiber Reinforced Cement Composites*, Vol.1.

Tepfers, R. 1973. *A theory of bond applied to overlapped tensile reinforcement splices for deformed bars*. Chalmers Univ. of Technology, Goteborg, Publ. 73/2, 328 pp.

van Mier, J.G.M. & Vervuurt, A. 1995. Lattice model for analysing steel-concrete interface behaviour. In A.P.S. Salvadurai and M.J. Boulon (eds), *Mechanics of Geomaterial Interfaces*: 201-225. Elsevier Science.

Yankelevsky D.Z. 1985. New finite element for bond-slip analysis. *ASCE Journal of Structural Engineering* 111(7): 1533-1542.